



In vivo quantification of bone mineral density of lumbar vertebrae using fast kVp switching dual-energy CT: correlation with quantitative computed tomography

Shuwei Zhou^{1,2#}, Lu Zhu^{3#}, Tian You¹, Ping Li¹, Hongrong Shen¹, Yewen He¹, Hui Gao¹, Luyou Yan¹, Zhuo He¹, Ying Guo¹, Yaxi Zhang¹, Kun Zhang^{1,2}

¹Department of Radiology, First Affiliated Hospital of Hunan University of Chinese Medicine, Changsha, China; ²The College of Integrated Traditional Chinese and Western Medicine, Hunan University of Chinese Medicine, Changsha, China; ³Department of Ultrasonography, Hunan Provincial People's Hospital, First Affiliated Hospital of Hunan Normal University, Changsha, China

#These authors contributed equally to this work.

Correspondence to: Kun Zhang, MD. Department of Radiology, First Affiliated Hospital of Hunan University of Chinese Medicine, 95 Shaoshan Middle Road, Yuhua District, Changsha 410007, China; the College of Integrated Traditional Chinese and Western Medicine, Hunan University of Chinese Medicine, 300 Xueshi Road, Yuelu District, Changsha 410208, China. Email: kun_zhang0102@163.com.

Background: Osteoporosis is a common, progressive disease related to low bone mineral density (BMD). If it can be diagnosed at an early stage, osteoporosis is treatable. Quantitative computed tomography (QCT) is one of the current reference standards of BMD measurement, but dual-energy computed tomography (DECT) is considered to be a potential alternative. This study aimed to evaluate the feasibility and accuracy of phantomless *in vivo* DECT-based BMD quantification in comparison with QCT.

Methods: A total of 128 consecutive participants who underwent DECT lumbar examinations between July 2018 and February 2019 were retrospectively analyzed. The density of calcium (water), hydroxyapatite (water), calcium (fat), and hydroxyapatite (fat) [$D_{Ca(Wa)}$, $D_{HAP(Wa)}$, $D_{Ca(Fat)}$ and $D_{HAP(Fat)}$, respectively] were measured along with BMD in the trabecular bone of lumbar level 1–2 by DECT and QCT. Linear regression analysis was performed to assess the relationship between DECT- and QCT-derived BMD at both the participant level and the vertebral level. Linear regression models were quantitatively evaluated with adjusted *R*-square, normalized mean squared error (NMSE) and relative error (RE). Bland-Altman analysis was conducted to assess agreement between measurements. $P < 0.05$ was considered statistically significant.

Results: Strong correlations were observed between DECT- and QCT-derived BMD at both the participant level and the vertebral level (adjusted $R^2 = 0.983–0.987$; NMSE = 1.6–2.1%; $RE_{linear} = 0.6–0.9\%$). Bland-Altman plots indicated high agreement between both measurements. $D_{Ca(Fat)}$ and $D_{HAP(Fat)}$ showed relatively similar and optimal predictive capability for QCT-derived BMD (both: adjusted $R^2 = 0.987$, NMSE = 1.6%, $RE_{linear} = 0.6\%$).

Conclusions: Fast kVp switching DECT enabled accurate phantomless *in vivo* BMD quantification of the lumbar spine. $D_{Ca(Fat)}$ and $D_{HAP(Fat)}$ had relatively similar and optimal predictive capability.

Keywords: Bone density; lumbar vertebrae; osteoporosis; tomography; X-ray computed

Submitted Feb 28, 2020. Accepted for publication Sep 16, 2020.

doi: 10.21037/qims-20-367

View this article at: <http://dx.doi.org/10.21037/qims-20-367>

Introduction

Osteoporosis is a common disease that causes low bone mass and bone microstructural destruction. Patients with osteoporosis have increased bone fragility and a high risk of fracture, which results in substantial family and socioeconomic burdens (1,2). Bone mineral density (BMD) is the main measurement of the amount of bone and is directly related to osteoporosis (3-5). Both dual-energy X-ray absorptiometry (DXA) and quantitative computed tomography (QCT) are regarded as reference standards for the measurement of BMD. DXA is used to measure the areal BMD (aBMD) in units of g/cm^2 . However, the early changes in bone mass in osteoporosis first occur in trabecular bone, due to the inner trabecular bone being more active metabolically and thus more sensitive to changes in BMD (6).

QCT has some advantages over DXA because of its three-dimensional nature and the opportunistic exploitation of routine CT scans. In recent years, QCT has increasingly been used instead of DXA to assess BMD of the lumbar spine (7,8). Uniquely, QCT can provide separate BMD values for trabecular and cortical bone and measure true volumetric BMD (vBMD) in units of mg/cm^3 (9,10), which not only reflects changes of bone mineral content in the vertebrae more accurately than DXA, but also predicts incident vertebral fractures more accurately than DXA (11-13). Phantomless QCT is gaining in popularity due to the convenience of requiring no calibration phantoms and the benefit of allowing for opportunistic BMD measurements. Currently, there are three main techniques of phantomless QCT. The first technique uses values of internal tissues (muscle and fat) as references for calibration when calculating BMD; the second allows for measurement of BMD without a phantom being scanned with each patient, as long as the CT modality is calibrated periodically; and the third estimates BMD by performing material decomposition (MD) using dual-energy CT (DECT) (14).

The recently introduced DECT method provides not only monochromatic images, but also accurate MD images by gemstone spectral imaging (GSI) (15,16). *In vivo* BMD can be estimated by quantifying the base materials using MD algorithms. Like QCT, DECT can also support separate measurements of the BMD of cortical and trabecular bone (5). Notably, the radiation exposure dose of DECT with the volume-based adaptive statistical iterative reconstruction (ASiR-V) technique is equal to or lower than

that of conventional CT (17-19). DECT also has other potential advantages, including detection of bone marrow edema or tumor infiltration. Compared with the first two techniques of phantomless QCT using conventional CT, DECT with the ASiR-V technique has no barriers to its use as a routine scan for lumbar examination, which suggests a promising future for BMD quantitation based on DECT.

Previous studies on the measurement of BMD by DECT are controversial and inadequate. van Hamersvelt *et al.* found a strong correlation between BMD measured by DECT and DXA (20), but their study was based on phantoms rather than patients. Conversely, other studies indicated a lack of correlation between DECT-derived and DXA-derived BMD, although these studies included fewer than 50 participants (21,22). Mei *et al.* reported that compared with QCT, DECT-based hydroxyapatite (HAP)-specific BMD quantitation had a high level of accuracy *in vitro* (23); however, its performance *in vivo* has yet to be evaluated. Recently, Roski *et al.* demonstrated the feasibility of phantomless *in vivo* dual-layer DECT-based HAP-specific BMD assessment, although only 33 patients were included and only HAP-specific BMD was measured (24). To date, few studies have investigated the use of the new-generation fast kVp switching DECT.

Some studies have demonstrated that absorption by any type of tissue can be determined by the proportions of its base materials, and with appropriate selection of the base materials their densities can reflect the content of the actual material in the tissue (19,25,26). The main components of the vertebral body include bone minerals (HAP/calcium), water, red marrow, yellow marrow (mainly fat), and collagen. Therefore, we hypothesized that compared with phantom-calibrated QCT, 256-row fast kVp switching DECT was feasible and accurate for phantomless BMD quantification *in vivo*. In our study, the density of four base material pairs were evaluated: calcium (water) [$D_{\text{Ca}(\text{Wa})}$]; HAP (water) [$D_{\text{HAP}(\text{Wa})}$]; calcium (fat) [$D_{\text{Ca}(\text{Fat})}$]; and HAP (fat) [$D_{\text{HAP}(\text{Fat})}$].

Methods

Study design and selection of subjects

Our study was approved by the institutional ethics committee of the First Affiliated Hospital of Hunan University of Chinese Medicine (no. HN-LL-KY-2019003016). Owing to the retrospective nature of this study, the requirement for informed consent was

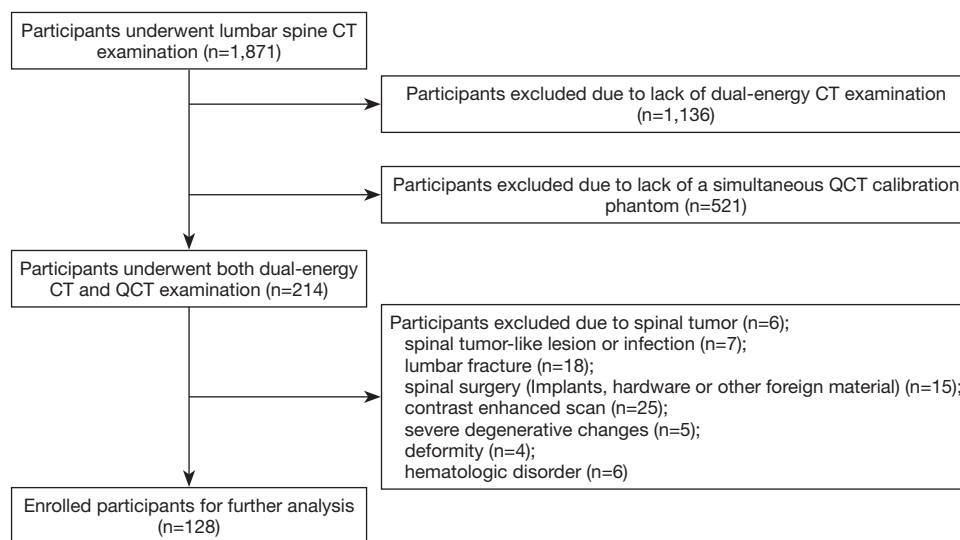


Figure 1 Flow chart according to the Standards for Reporting of Diagnostic Accuracy Studies.

waived. Data from subjects who underwent DECT lumbar examinations between July 2018 and February 2019 were collected. The subjects' demographic characteristics [age, sex, and body mass index (BMI)] before scanning were recorded. The exclusion criteria were no simultaneous QCT calibration phantom; spinal tumor; spinal tumor-like lesions or infection; lumbar fracture; spinal surgery (implants, hardware, or other foreign material); contrast-enhanced scan; severe degenerative changes; deformity; and hematologic disorder (12,14). Finally, 128 consecutive participants were enrolled. *Figure 1* is a flowchart of the study following the guidelines of Standards for Reporting of Diagnostic Accuracy. The sample size consideration is shown in [Supplementary Material A1](#).

DECT and phantom-calibrated QCT scan protocols

In our study, all lumbar examinations of the enrolled participants were performed simultaneously with a bone density calibration (BDC) phantom placed beneath the spine, to avoid additional radiation exposure. CT imaging of the spine was performed with a Revolution GSI CT scanner (GE Medical Systems, Milwaukee, WI, USA). *Table 1* shows the detailed scanning parameters of DECT, and [Supplementary Material A2](#) shows the radiation exposure dose consideration of DECT using the ASiR-V technique (27).

The BDC phantom (QRM, Moehrendorf, Germany) contained 6 cylindrical inserts, each with a diameter of

1.8 cm and an exact value of 0, 98.8, 201.9, 390.5, 599.1, and 793.7 mg/cm³ HAP, respectively. All phantom-calibrated QCT analyses were performed according to the ISCD consensus, and BMD was measured at L1 (lumbar level 1) and L2 (lumbar level 2) (13). The DECT scanner undergoes a 'fast calibration' protocol every week to ensure correct CT values of water and no artifacts. The accuracy and precision of the QCT devices based on DECT are tested every week using the same scan protocol (for details see [Supplementary Material A3](#)).

Post-processing of DECT and phantom-calibrated QCT image data

The MD data and QCT data were evaluated in random order by Y.H. (8 years of experience in musculoskeletal radiology) and H.G. (10 years of experience), respectively, who were independent and blinded to each other's results. The raw image data were transmitted to an advanced workstation (ADW4.6; GE Medical Systems). As they had lower image noise and a higher contrast-to-noise ratio (CNR) than 120-kVp CT images, but equal CT values, 70-keV monochromatic images were used to measure the CT values of both the vertebrae and the phantom in this study (28,29). The reproducibility and accuracy of spinal QCT using different scan protocols is shown in [Supplementary Material A3](#) and *Table S1*.

For further analysis, 5-mm axial images were viewed. In the central level of the lumbar vertebral body, the region

Table 1 Scanning parameters of dual-energy CT

CT parameters	Details
Mode	GSI helical
Rotation speed (s/rot)	0.8
Pitch	0.984:1
Tube voltage (kVp)	80/140
Tube current (mA)	230
Beam collimation (mm)	256×0.625
ASiR-V	30%
Recon type	Bone
CTDIvol (mGy)	9.09

ASiR-V, volume-based adaptive statistical iterative reconstruction; CTDIvol, volume computed tomography dose index; GSI, gemstone spectral imaging.

of interest (ROI) was drawn along the inner edge of the vertebral body to calculate the average CT attenuation value (HU), avoiding the cortical bone and the vertebral venous plexuses posteriorly (*Figure 2*). $D_{Ca(Wa)}$, $D_{HAP(Wa)}$, $D_{Ca(Fat)}$, and $D_{HAP(Fat)}$ were also separately measured in the MD images. The main component of bone is HAP [chemical formula $Ca_{10}(PO_4)_6(OH)_2$]. The relative atomic weight of calcium (Ca) is 40. Because there are 10 Ca atoms in HAP, the amount of Ca is 400, and the relative molecular weight of HAP is 1,004. When the Ca content of HAP is known, the HAP content can be estimated according to Eq. [1]. A circular ROI with a fixed diameter of 10 mm was marked in the center of each insert in the BDC phantom, and the mean CT number of each insert was measured (*Figure 2*). A linear regression Eq. [2] could be calculated with the known HAP content and CT attenuation value of each insert in the phantom, and then the CT attenuation value of the vertebral body could be converted into BMD through Eq. [2] (23).

$$BMD_{GSI} = \rho_{Ca-H_2O(Fat)} \times 1004/400 \quad [1]$$

$$BMD = \beta \cdot CT \text{ attenuation value} + c \quad [2]$$

ρ_{Ca-H_2O} and ρ_{Ca-Fat} are the density of calcium (water) and calcium (fat), respectively.

β and c are the coefficient and intercept of the linear formula, respectively.

Statistical analysis

SPSS statistical analysis software (v.20.0; IBM) and R software (version 3.5.1; <http://www.Rproject.org>) were used

for statistical analysis. Continuous variables were compared using the Wilcoxon test or Student's t test. The data were checked for homogeneity and normality using the Levene's and Shapiro-Wilk tests, respectively.

Linear regression analysis was used to assess the relationship between DECT- and QCT-derived BMD. Linear regression models were quantitatively evaluated using adjusted R-square, normalized mean squared error (NMSE), and relative error (RE) (30,31). NMSE was calculated by 10-fold cross-validation, according to Eq. [3]:

$$NMSE = \frac{\sum(y_i - \hat{y}_i)^2}{\sum(y_i - \bar{y})^2} \quad [3]$$

y_i is the true value of BMD in test set, \hat{y}_i is the predicted value of BMD in test set, \bar{y} is the mean of true value of BMD in test set.

RE was calculated in two ways according to Eq. [4]:

$$RE = \Delta/L \times 100\% \quad [4]$$

RE is generally given as a percentage, Δ -Absolute error (predicted value minus true value), and L -True value (QCT-derived BMD). For RE_{linear} , the adjusted predicted BMD from the linear regression model was used to calculate Δ . The adjusted predicted value for a case is the predicted value when that case is excluded from the calculation of the regression coefficients (corresponding to leave-one-out cross-validation). For RE_{direct} , the D_{HAP} (D_{Ca} converted into D_{HAP}) measured in MD images was considered as the predicted value to calculate Δ .

Bland-Altman analysis was conducted to assess agreement between the adjusted predicted BMD (derived from linear regression calibration) and QCT-derived BMD (32).

Statistical significance was indicated by two-sided $P < 0.05$.

Results

Characteristics of the subjects

The demographic characteristics of the subjects are summarized in *Table 2*. The data were analyzed at both the participant level ($n=128$, the average of L1–L2 per participant was used for analysis) and the vertebral level ($n=128$, L1 and L2, separately).

Relationship between QCT-derived and DECT-derived BMD

The results of this section are summarized in *Figures 3* and *4*, and *Table S2*.

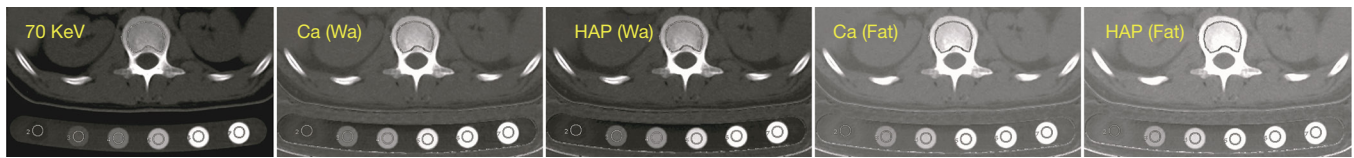


Figure 2 Vertebral bodies and phantom as shown in 70-KeV monochromatic images and four types of material decomposition (MD) images. U-shaped areas illustrate the regions-of-interest (ROI) in the L1 vertebral bodies, and circles illustrate ROI placement in the QCT phantom.

Table 2 Demographic characteristics [mean \pm standard deviation (SD)]

Characteristic	Male (n=62)	Female (n=66)	P value
Age (years)	51.31 \pm 17.67	51.98 \pm 18.39	0.830
BMI (kg·cm ⁻²)	23.40 \pm 3.65	21.63 \pm 3.08	0.003
BMD (mg/cm ³)	126.84 \pm 48.78	118.95 \pm 55.53	0.396
L1	128.08 \pm 49.65	121.31 \pm 53.43	0.460
L2	125.61 \pm 48.36	116.59 \pm 58.29	0.340

BMD, bone mineral density; BMI, body mass index.

The results for the participant level are as follows. The RE_{direct} of $D_{\text{Ca(Wa)}}$, $D_{\text{HAP(Wa)}}$, $D_{\text{Ca(Fat)}}$, and $D_{\text{HAP(Fat)}}$ was -56.7% , -63.2% , -37.5% , and -47.8% , respectively. *Figure 3* shows the significant positive correlations between the densities of the four base materials [$D_{\text{Ca(Wa)}}$, $D_{\text{HAP(Wa)}}$, $D_{\text{Ca(Fat)}}$ and $D_{\text{HAP(Fat)}}$] and QCT-derived BMD ($R=0.992\text{--}0.993$, adjusted $R^2=0.985\text{--}0.987$, all $P<0.001$). All the linear models showed good predictive capability of BMD (NMSE = $1.6\text{--}1.8\%$, $RE_{\text{linear}}=0.6\text{--}0.7\%$).

Additionally, the agreements between BMD measurements based on linear regression calibrated DECT and QCT were assessed with Bland-Altman plots (*Figure 4*). For all four base materials, the mean differences were zero (all $P>0.05$); most of the differences lay between ± 1.96 SD, and there were no clear trends, which indicated high agreement between both measurements.

The results for the vertebral level were as good as those based on the participant level. The densities of the four base materials [$D_{\text{Ca(Wa)}}$, $D_{\text{HAP(Wa)}}$, $D_{\text{Ca(Fat)}}$, and $D_{\text{HAP(Fat)}}$] and QCT-derived BMD were highly correlated ($R=0.991\text{--}0.993$, adjusted $R^2=0.983\text{--}0.987$, all $P<0.001$). All of the linear models showed good predictive capability of BMD (NMSE = $1.7\text{--}2.1\%$, $RE_{\text{linear}}=0.7\text{--}0.9\%$).

All of the above results indicated the robustness and accuracy of our models. Furthermore, $D_{\text{Ca(Fat)}}$ and $D_{\text{HAP(Fat)}}$ were found to demonstrate relatively similar and optimal

predictive capability for QCT-derived BMD (both: adjusted $R^2=0.987$, NMSE = 1.6% , $RE_{\text{linear}}=0.6\%$).

Discussion

Osteoporosis is a chronic condition that imposes significant health, social, and economic burdens worldwide because of its prevalence. However, with early medical intervention, the condition can be treated. Consequently, early diagnosis of osteoporosis has attracted considerable attentions (1). Our study demonstrated that fast kVp switching DECT enabled accurate BMD quantification of the lumbar spine *in vivo* without the need for phantom-calibration, and the $D_{\text{Ca(Fat)}}$ -specific and $D_{\text{HAP(Fat)}}$ -specific densities showed relatively similar and optimal predictive capability.

Controversy surrounds the associations between DECT-derived and DXA-derived BMD found in previous studies. Van Hamersvelt *et al.* inferred that DECT allowed accurate BMD quantification *in vitro* by using two validated anthropomorphic phantoms with material-specific known concentrations (20); Similarly, Wait *et al.* indicated that DECT was more sensitive than DXA in detecting changes of BMD, and that the BMD values measured by DECT and DXA were highly correlated (5). On the other hand, DECT-derived and DXA-derived BMD values have been reported to have a low correlation. In the study by Wesarg

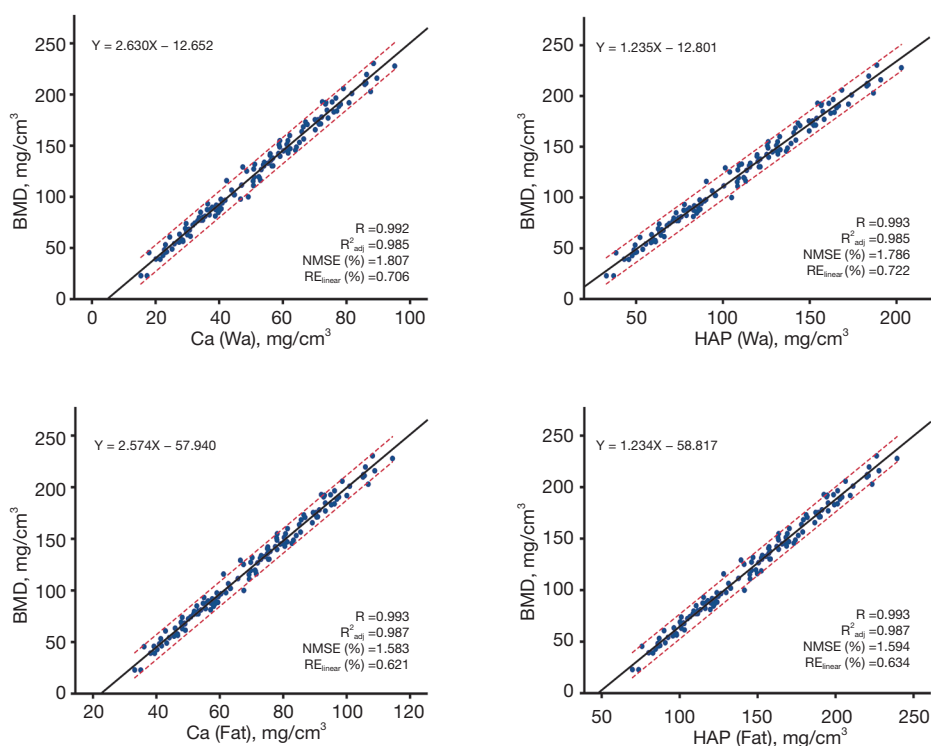


Figure 3 Associations between the densities of the four base materials and QCT-derived BMD at the participant level. Straight black lines indicate lines of best fit. Dotted red lines indicate 95% confidence interval for individual prediction intervals. Plots indicate high correlations ($R > 0.99$, adjusted $R^2 > 0.98$ for all), along with good predictive capability of BMD ($NMSE < 1.9\%$, $RE_{linear} < 0.8\%$ for all). BMD, bone mineral density; QCT, quantitative computed tomography; R, correlation coefficient; R^2_{adj} , adjusted coefficient of determination; NMSE, normalized mean squared error; RE, relative error.

et al., 29 cadaver specimens were evaluated, and the authors observed only a moderate linear correlation of the BMD measurements between DECT and DXA (33). Moreover, Wichmann *et al.* analyzed 160 lumbar vertebrae in 40 participants and reported a lack of correlation between the BMD results derived from DECT and DXA (21). In our study, with QCT serving as the reference standard, strong linear correlations were observed between the densities of the four base materials [$D_{Ca(Wa)}$, $D_{HAP(Wa)}$, $D_{Ca(Fat)}$ and $D_{HAP(Fat)}$] and phantom-calibrated BMD.

There are several possible reasons for the discrepancies among studies. Firstly, DXA measures aBMD in g/cm^2 , but QCT measures vBMD in mg/cm^3 , which allows for differentiation of trabecular and cortical bone. Secondly, the results of the studies conducted on phantoms were better than those of the studies conducted on participants, which might relate to fewer interfering factors in the phantom studies, such as individual patient differences. Thirdly, our research was conducted on 128 participants of different

sexes, ages, and BMI from a clinic, but only 40 participants were included in the study by Wichmann *et al.*, which makes our results more reliable. Fourthly, we used DECT with the new generation of spectral imaging technology in MD; this gave wider detector coverage, better image quality, and lower exposure dosage, all of which are helpful for accurate quantification of BMD. In general, the results of our study may be more accurate and convincing.

Recently, Mei *et al.* demonstrated that with a radiation exposure of ≥ 50 mAs, a high correlation was found between BMD values measured with DECT and QCT (23,24). They investigated BMD quantitation both in phantoms with known HAP concentrations and in participants, showing the measurements to be highly accurate. Taken together, the findings suggest that phantomless BMD quantitation based on DECT imaging is feasible and could be applied clinically. It must be emphasized that our study was conducted on the lumbar vertebrae of 128 participants, and the densities of four base material pairs [$D_{Ca(Wa)}$,

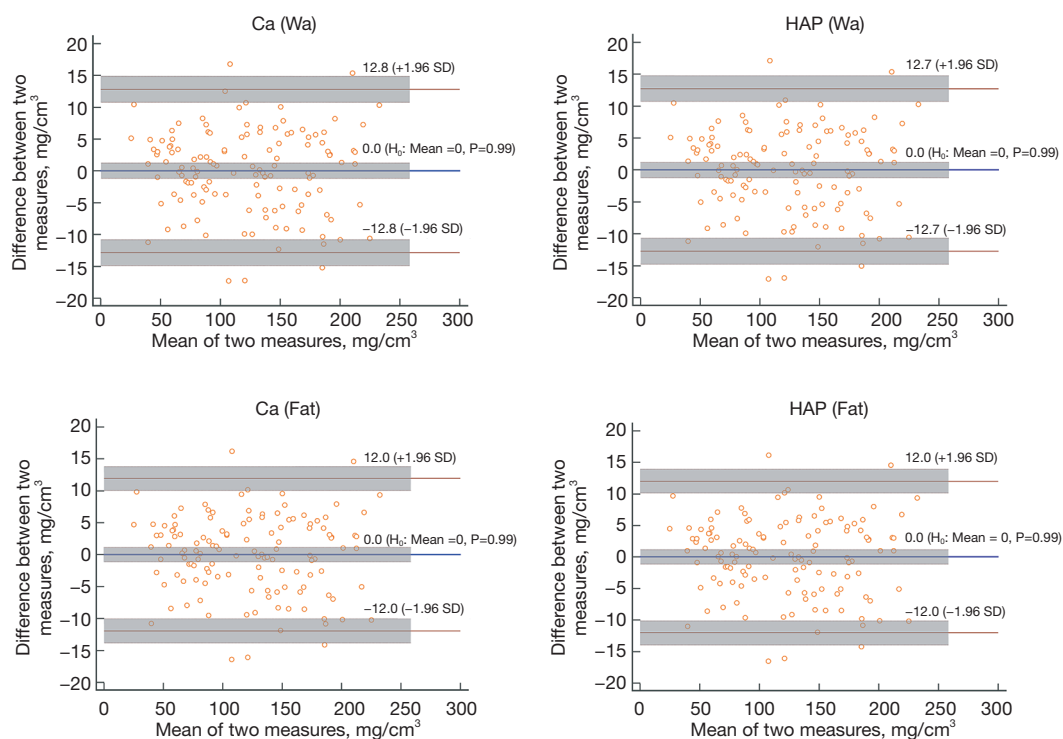


Figure 4 Bland-Altman plots at the participant level show the differences of BMD measurements between linear regression calibrated dual-energy CT and QCT versus the means of the two methods separately for different material decomposition techniques. Normal distribution of the differences was verified with Shapiro–Wilk test (all $P > 0.05$). Solid blue lines indicate mean BMD differences; solid red lines indicate mean differences ± 1.96 SD (agreement limits); shaded areas indicate 95% confidence interval limits for mean differences and agreement limits. As all mean differences were zero (all $P > 0.05$), most of the differences lay between ± 1.96 SD, and there were no clear trends found along the graphs, Bland-Altman plots indicate high agreement between both measurements.

$D_{\text{HAP(Wa)}}$, $D_{\text{Ca(Fat)}}$ and $D_{\text{HAP(Fat)}}$ were analyzed, with significant correlations found between BMD values measured by DECT and QCT. Our results suggest that material-specific measurements are an adequate alternative for the detection of patients with low BMD in routine clinical practice.

Few studies have investigated the relationship between BMD predictive capability and different MD technology. Several methods (adjusted R^2 , RE, and NMSE) were applied in the linear model evaluation in this study, and good linearity, stability and consistency were shown at both the participant level and the vertebral level. Furthermore, $D_{\text{Ca(Fat)}}$ and $D_{\text{HAP(Fat)}}$ had relatively similar and optimal predictive capability. Materials display energy-dependent X-ray absorption at different kilovoltage peak levels. With DECT, materials can be further differentiated through the differences in attenuation by applying different X-ray spectra (34–36). Our results indicated that the stability of the MD technique for the four-base material pairs may

differ. However, the stability was relatively similar and optimal between Ca(Fat) and HAP(Fat), which brought the most accurate BMD predictive results calibrated by regression equation.

To date, there have been two methods of predicting BMD by DECT: direct quantification based on measurements in MD images, and indirect quantification through linear regression calibration. However, few studies have compared the accuracy of these methods. It is interesting that the direct quantification method was not as accurate as we expected. The REs of the four-base material pairs in the direct method were large and varied, which would result in biased estimates and makes the method difficult to apply clinically. In contrast, the REs of the four-base material pairs with the indirect method were small and similar, and the agreement between the indirect method and QCT was good, which implied great clinical value. These results demonstrated that the DECT MD should

not be considered as a measurement of the true content of a certain material, but only reflects the relative content and the change trend of the base materials. The estimated values of the direct method needed to be calibrated by linear regression equation for clinical use.

Study limitations

This study has some limitations that need to be addressed. Firstly, there are various components of the vertebral body [red marrow, yellow marrow (mainly fat), water, collagen, and bone minerals] and the present noninvasive BMD/fat quantification methods, including DECT, DXA, conventional QCT, and MRI, can only provide rough estimates. However, chemically analyzed density measurement is not applicable *in vivo*. Secondly, only the lumbar spine was analyzed in this study, and the values for the thoracic vertebrae, proximal femur, and distal radius, which are also at risk of fragility fractures, should be considered. Thus, in future study, we will aim to address predictive capability of the BMD in those sites.

In conclusion, 256-row dual-energy CT with fast kVp switching technique enabled accurate *in vivo* BMD quantification of lumbar spine without phantom-calibration. $D_{Ca(Fat)}$ and $D_{HAP(Fat)}$ had relatively similar and optimal predictive capability, which may open up the possibilities of using this DECT technique for osteoporosis assessment in clinical practice.

Acknowledgments

Funding: This work was supported by National Natural Science Foundation of China (grant no. 81603482), Hunan Natural Science Foundation (grant no. 2016JJ6115), China Postdoctoral Science Foundation (grant no. 2017M622586), Key Discipline Construction Project of Hunan University of Chinese Medicine (grant no. 4901-020000200806).

Footnote

Conflicts of Interest: All authors have completed the ICMJE uniform disclosure form (available at <http://dx.doi.org/10.21037/qims-20-367>). The authors have no conflicts of interest to declare.

Ethical Statement: The study was conducted in accordance with the Declaration of Helsinki (as revised in 2013). Ethics approval for this study was given by the institutional

ethics committee of the First Affiliated Hospital of Hunan University of Chinese Medicine (no. HN-LL-KY-2019003016), and the requirement for informed consent was waived.

Open Access Statement: This is an Open Access article distributed in accordance with the Creative Commons Attribution-NonCommercial-NoDerivs 4.0 International License (CC BY-NC-ND 4.0), which permits the non-commercial replication and distribution of the article with the strict proviso that no changes or edits are made and the original work is properly cited (including links to both the formal publication through the relevant DOI and the license). See: <https://creativecommons.org/licenses/by-nc-nd/4.0/>.

References

1. Brown C. Osteoporosis: Staying strong. *Nature* 2017;550:S15-7.
2. Sánchez-Riera L, Carnahan E, Vos T, Veerman L, Norman R, Lim SS, Hoy D, Smith E, Wilson N, Nolla JM, Chen JS, Macara M, Kamalaraj N, Li Y, Kok C, Santos-Hernandez C, March L. The global burden attributable to low bone mineral density. *Ann Rheum Dis* 2014;73:1635-45.
3. Berry SD, Samelson EJ, Pencina MJ, McLean RR, Cupples LA, Broe KE, Kiel DP. Repeat bone mineral density screening and prediction of hip and major osteoporotic fracture. *Jama* 2013;310:1256-62.
4. Wu Y, Guo Z, Fu X, Wu J, Gao J, Zeng Q, Fu H, Cheng X. The study protocol for the China Health Big Data (China Biobank) project. *Quant Imaging Med Surg* 2019;9:1095-102.
5. Wait JM, Cody D, Jones AK, Rong J, Baladandayuthapani V, Kappadath SC. Performance Evaluation of Material Decomposition With Rapid-Kilovoltage-Switching Dual-Energy CT and Implications for Assessing Bone Mineral Density. *AJR Am J Roentgenol* 2015;204:1234-41.
6. Engelke K, Adams JE, Armbrrecht G, Augat P, Bogado CE, Bouxsein ML, Felsenberg D, Ito M, Prevrhal S, Hans DB, Lewiecki EM. Clinical use of quantitative computed tomography and peripheral quantitative computed tomography in the management of osteoporosis in adults: the 2007 ISCD Official Positions. *J Clin Densitom* 2008;11:123-62.
7. Link TM, Lang TF. Axial QCT: clinical applications and new developments. *J Clin Densitom* 2014;17:438-48.
8. Gerety EL, Hopper MA, Bearcroft PW. The reliability

- of measuring the density of the L1 vertebral body on CT imaging as a predictor of bone mineral density. *Clin Radiol* 2017;72:177.e9-15.
9. Liu Y, Carrino JA, Dash AS, Chukir T, Do H, Bockman RS, Hughes AP, Press JM, Stein EM. Lower Spine Volumetric Bone Density in Patients With a History of Epidural Steroid Injections. *J Clin Endocrinol Metab* 2018;103:3405-10.
 10. Kwon D, Kim J, Lee H, Kim B, Han H, Oh H, Kim M, Yoon H, Lee B, Eom K. Quantitative computed tomographic evaluation of bone mineral density in beagle dogs: comparison with dual-energy x-ray absorptiometry as a gold standard. *J Vet Med Sci* 2018;80:620-8.
 11. Black DM, Bouxsein ML, Marshall LM, Cummings SR, Lang TF, Cauley JA, Ensrud KE, Nielson CM, Orwoll ES. Proximal femoral structure and the prediction of hip fracture in men: a large prospective study using QCT. *J Bone Miner Res* 2008;23:1326-33.
 12. Löffler MT, Jacob A, Valentinitisch A, Rienmüller A, Zimmer C, Ryang YM, Baum T, Kirschke JS. Improved prediction of incident vertebral fractures using opportunistic QCT compared to DXA. *Eur Radiol* 2019;29:4980-9.
 13. Shuhart CR, Yeap SS, Anderson PA, Jankowski LG, Lewiecki EM, Morse LR, Rosen HN, Weber DR, Zemel BS, Shepherd JA. Executive Summary of the 2019 ISCD Position Development Conference on Monitoring Treatment, DXA Cross-calibration and Least Significant Change, Spinal Cord Injury, Peri-prosthetic and Orthopedic Bone Health, Transgender Medicine, and Pediatrics. *Journal of Clinical Densitometry* 2019;22:453-71.
 14. American College of Radiology (2018) ACR-SPR-SSR practice parameter for the performance of musculoskeletal quantitative computed tomography (QCT). Available online: <https://www.acr.org/-/media/ACR/Files/Practice-Parameters/QCT.pdf>, Accessed 7 Nov 2018.
 15. Pan J, Yan L, Gao H, He Y, Zhong Z, Li P, Zhang Y, Guo Y, Liao L, Zhou S, Zhang K. Fast kilovoltage (KV)-switching dual-energy computed tomography hydroxyapatite (HAP)-water decomposition technique for identifying bone marrow edema in vertebral compression fractures. *Quant Imaging Med Surg* 2020;10:604-11.
 16. Mallinson PI, Coupal TM, McLaughlin PD, Nicolaou S, Munk PL, Ouellette HA. Dual-Energy CT for the Musculoskeletal System. *Radiology* 2016;281:690-707.
 17. Li W, Li A, Wang B, Niu X, Cao X, Wang X, Shi H. Automatic spectral imaging protocol and iterative reconstruction for radiation dose reduction in typical hepatic hemangioma computed tomography with reduced iodine load: a preliminary study. *Br J Radiol* 2018;91:20170978.
 18. Lv P, Zhou Z, Liu J, Chai Y, Zhao H, Guo H, Marin D, Gao J. Can virtual monochromatic images from dual-energy CT replace low-kVp images for abdominal contrast-enhanced CT in small- and medium-sized patients? *Eur Radiol* 2019;29:2878-89.
 19. Zheng S, Dong Y, Miao Y, Liu A, Zhang X, Wang B, Ge Y, Liu Y, Wang S. Differentiation of osteolytic metastases and Schmorl's nodes in cancer patients using dual-energy CT: advantage of spectral CT imaging. *Eur J Radiol* 2014;83:1216-21.
 20. van Hamersvelt RW, Schilham AMR, Engelke K, den Harder AM, de Keizer B, Verhaar HJ, Leiner T, de Jong PA, Willeminck MJ. Accuracy of bone mineral density quantification using dual-layer spectral detector CT: a phantom study. *Eur Radiol* 2017;27:4351-9.
 21. Wichmann JL, Booz C, Wesarg S, Kafchitsas K, Bauer RW, Kerl JM, Lehnert T, Vogl TJ, Khan MF. Dual-energy CT-based phantomless in vivo three-dimensional bone mineral density assessment of the lumbar spine. *Radiology* 2014;271:778-84.
 22. Booz C, Hofmann PC, Sedlmair M, Flohr TG, Schmidt B, D'Angelo T, Martin SS, Lenga L, Leithner D, Vogl TJ, Wichmann JL. Evaluation of bone mineral density of the lumbar spine using a novel phantomless dual-energy CT post-processing algorithm in comparison with dual-energy X-ray absorptiometry. *Eur Radiol Exp* 2017;1:11.
 23. Mei K, Schwaiger BJ, Kopp FK, Ehn S, Gersing AS, Kirschke JS, Muenzel D, Fingerle AA, Rummeny EJ, Pfeiffer F, Baum T, Noel PB. Bone mineral density measurements in vertebral specimens and phantoms using dual-layer spectral computed tomography. *Sci Rep* 2017;7:17519.
 24. Roski F, Hammel J, Mei K, Baum T, Kirschke JS, Laugerette A, Kopp FK, Bodden J, Pfeiffer D, Pfeiffer F, Rummeny EJ, Noël PB, Gersing AS, Schwaiger BJ. Bone mineral density measurements derived from dual-layer spectral CT enable opportunistic screening for osteoporosis. *Eur Radiol* 2019;29:6355-63.
 25. Dong Y, Zheng S, Machida H, Wang B, Liu A, Liu Y, Zhang X. Differential diagnosis of osteoblastic metastases from bone islands in patients with lung cancer by single-source dual-energy CT: advantages of spectral CT imaging. *Eur J Radiol* 2015;84:901-7.
 26. Fischer MA, Gnannt R, Raptis D, Reiner CS, Clavien PA,

- Schmidt B, Leschka S, Alkadhi H, Goetti R. Quantification of liver fat in the presence of iron and iodine: an ex-vivo dual-energy CT study. *Invest Radiol* 2011;46:351-8.
27. Marin D, Nelson RC, Schindera ST, Richard S, Youngblood RS, Yoshizumi TT, Samei E. Low-tube-voltage, high-tube-current multidetector abdominal CT: improved image quality and decreased radiation dose with adaptive statistical iterative reconstruction algorithm--initial clinical experience. *Radiology* 2010;254:145-53.
 28. Matsumoto K, Jinzaki M, Tanami Y, Ueno A, Yamada M, Kuribayashi S. Virtual monochromatic spectral imaging with fast kilovoltage switching: improved image quality as compared with that obtained with conventional 120-kVp CT. *Radiology* 2011;259:257-62.
 29. Yamada Y, Jinzaki M, Hosokawa T, Tanami Y, Abe T, Kuribayashi S. Abdominal CT: an intra-individual comparison between virtual monochromatic spectral and polychromatic 120-kVp images obtained during the same examination. *Eur J Radiol* 2014;83:1715-22.
 30. Engelke K, Glüer CC. Quality and performance measures in bone densitometry: part 1: errors and diagnosis. *Osteoporos Int* 2006;17:1283-92.
 31. Chen KY. Combining linear and nonlinear model in forecasting tourism demand. *Expert Systems with Applications* 2011;38:10368-76.
 32. Bland JM, Altman DG. Statistical methods for assessing agreement between two methods of clinical measurement. *Lancet* 1986;1:307-10.
 33. Wesarg S, Kirschner M, Becker M, Erdt M, Kafchitsas K, Khan MF. Dual-energy CT-based assessment of the trabecular bone in vertebrae. *Methods Inf Med* 2012;51:398-405.
 34. Johnson TR, Krauss B, Sedlmair M, Grasruck M, Bruder H, Morhard D, Fink C, Weckbach S, Lenhard M, Schmidt B, Flohr T, Reiser MF, Becker CR. Material differentiation by dual energy CT: initial experience. *Eur Radiol* 2007;17:1510-7.
 35. Sauter AP, Hammel J, Ehn S, Achterhold K, Kopp FK, Kimm MA, Mei K, Laugerette A, Pfeiffer F, Rummeny EJ, Pfeiffer D, Noel PB. Perfusion-ventilation CT via three-material differentiation in dual-layer CT: a feasibility study. *Sci Rep* 2019;9:5837.
 36. Yeh BM, Shepherd JA, Wang ZJ, Teh HS, Hartman RP, Pevrhal S. Dual-energy and low-kVp CT in the abdomen. *AJR Am J Roentgenol* 2009;193:47-54.

Cite this article as: Zhou S, Zhu L, You T, Li P, Shen H, He Y, Gao H, Yan L, He Z, Guo Y, Zhang Y, Zhang K. *In vivo* quantification of bone mineral density of lumbar vertebrae using fast kVp switching dual-energy CT: correlation with quantitative computed tomography. *Quant Imaging Med Surg* 2021;11(1):341-350. doi: 10.21037/qims-20-367

Table S1 Assessment of reproducibility and accuracy

	Insert 1	Insert 2	Insert 3	Insert 4	Insert 5
Brilliance					
BMD (mg/cm ³)	105.28±0.90	201.47±1.96	387.71±2.57	593.73±0.89	802.24±1.88
CV (%)	0.86	0.97	0.66	0.15	0.23
RE (%)	6.56±0.91	-0.21±0.97	-0.72±0.66	-0.90±0.15	1.08±0.24
Revolution					
BMD (mg/cm ³)	100.62±1.29	198.05±0.97	387.18±1.43	600.43±0.89	796.74±1.01
CV (%)	1.28	0.49	0.37	0.15	0.13
RE (%)	1.84±1.31	-1.91±0.48	-0.85±0.37	0.22±0.15	0.38±0.13

The exact value of inserts 1–5 was 98.8, 201.9, 390.5, 599.1, and 793.7 mg/cm³ hydroxyapatite (HAP), respectively. Bone mineral density (BMD) and relative error (RE) are expressed as mean ± SD. CV, coefficient of variation.

Table S2 Relationship between QCT-derived BMD and dual-energy CT-derived BMD

Subgroups	Base material pairs	N	R	R ² _{adj}	β	c	P	NMSE (%), mean (95% CI)	RE _{linear} (%), mean (95% CI)	RE _{direct} (%), mean (95% CI)
All (participant level)	Ca (Wa)	128	0.992	0.985	2.630	-12.652	<0.001	1.8 (1.2–2.4)	0.7 (-0.6–2.0)	-56.7 (-57.6–-55.8)
	HAP(Wa)	128	0.993	0.985	1.235	-12.801	<0.001	1.8 (1.2–2.4)	0.7 (-0.6–2.1)	-63.2 (-64.0–-62.5)
	Ca (Fat)	128	0.993	0.987	2.574	-57.940	<0.001	1.6 (1.1–2.1)	0.6 (-0.6–1.9)	-37.5 (-40.3–-34.7)
	HAP(Fat)	128	0.993	0.987	1.234	-58.817	<0.001	1.6 (1.1–2.1)	0.6 (-0.6–1.9)	-47.8 (-50.1–-45.4)
L1 (vertebral level)	Ca (Wa)	128	0.991	0.983	2.593	-10.649	<0.001	2.1 (1.5–2.7)	0.8 (-0.5–2.0)	-57.0 (-57.8–-56.3)
	HAP(Wa)	128	0.991	0.983	1.218	-11.038	<0.001	2.1 (1.4–2.7)	0.7 (-0.6–2.0)	-63.4 (-64.1–-62.8)
	Ca (Fat)	128	0.992	0.984	2.538	-55.341	<0.001	1.9 (1.3–2.4)	0.7 (-0.6–1.9)	-38.5 (-40.9–-36.0)
	HAP(Fat)	128	0.992	0.984	1.219	-56.479	<0.001	1.9 (1.3–2.5)	0.7 (-0.5–1.9)	-48.6 (-50.6–-46.5)
L2 (vertebral level)	Ca (Wa)	128	0.992	0.984	2.653	-13.888	<0.001	2.0 (1.3–2.7)	0.8 (-0.7–2.4)	-56.2 (-57.4–-55.0)
	HAP(Wa)	128	0.992	0.985	1.245	-13.835	<0.001	2.0 (1.3–2.6)	0.9 (-0.6–2.4)	-62.8 (-63.8–-61.8)
	Ca (Fat)	128	0.993	0.987	2.599	-59.673	<0.001	1.7 (1.1–2.3)	0.8 (-0.7–2.1)	-35.7 (-39.5–-31.8)
	HAP(Fat)	128	0.993	0.987	1.245	-60.300	<0.001	1.7 (1.1–2.3)	0.7 (-0.7–2.1)	-46.3 (-49.5–-43.0)

QCT, quantitative computed tomography; BMD, bone mineral density; N, sample size; R²_{adj}, adjusted R-square; β, coefficient of the linear formula; c, intercept of the linear formula; NMSE, normalized mean squared error; RE, relative error.

Supplementary Material A1 Sample size consideration

For linear regression, the rule of thumb usually adopted is that the sample size should be no less than 5–20-fold the number of variables (37). In our study, the number of variables was 1, and all the sample sizes were 128; thus, the sample sizes of our study were far more than the minimum sample size required.

Supplementary Material A2 Radiation exposure dose consideration

With advances in technology, the radiation exposure dose during the lumbar examination using dual-energy CT with ASiR-V technique is equal to or lower than that with conventional CT (17,18,27). To further validate this, the exposure dosage data for all adults who underwent conventional CT lumbar examinations during July 2018 were retrospectively collected. The conventional CT imaging of the lumbar spine was performed on a 64-multidetector CT scanner (Brilliance, Philips Healthcare, Eindhoven, The Netherlands). The scanning parameters included: 64 × 0.625 mm detector collimation, 1 s rotation time, 0.798 pitch, and 120 kVp tube voltage with tube current modulation (Z-DOM).

A total of 89 consecutive adults (44 males, age: 51.0±14.2 years; 45 females, age: 51.6±16.5 years) were enrolled. The CTDIvol during the lumbar examination using conventional CT was 17.5±3.7 mGy (range, 11.5–28.3 mGy).

In our institution, the CTDIvol during lumbar examinations with dual-energy CT and ASiR-V technique (9.09 mGy) is lower than that of conventional CT (17.5±3.7 mGy). Therefore, we believe that there should be no great concern about the radiation exposure dose in our study.

Supplementary Material A3 Reproducibility and accuracy consideration of spinal QCT using different scanning protocols

The BDC phantom (QRM, Moehrendorf, Germany) was separately scanned 10 times without repositioning using two CT scanners (256-row GE Revolution; 64-row Philips Brilliance). The scanning protocol for the Revolution CT scanner was the same as that used *in vivo* in the present study. The scanning protocol for the Brilliance CT scanner was: 64 × 0.625 mm detector collimation, 1 s rotation time, 0.798 pitch, and 120 kVp tube voltage with 125 mA tube current.

The 70-keV monochromatic images of the Revolution CT scanner were used to measure the CT values of the phantom. Using the linear calibration described in this study, the adjusted predicted BMD of the inserts in the BDC phantom were used for further analysis. The adjusted predicted value for a case is the predicted value when that case is excluded from the calculation of the regression coefficients. Accuracy and reproducibility are described as relative error (RE) and coefficient of variation (CV), respectively (30,38).

The reproducibility and accuracy of spinal QCT were assessed, and the results are shown in *Table S1*. Our results indicated that the reproducibility and accuracy of spinal QCT using 70-keV monochromatic data were equal to those of conventional spinal QCT (39,40).

References

37. Norman G, Monteiro S, Salama S. Sample size calculations: should the emperor's clothes be off the peg or made to measure? *BMJ* 2012;345:e5278.
38. Glüer CC, Blake G, Lu Y, Blunt BA, Jergas M, Genant HK. Accurate assessment of precision errors: how to measure the reproducibility of bone densitometry techniques. *Osteoporos Int* 1995;5:262-70.
39. Wu Y, Jiang Y, Han X, Wang M, Gao J. Application of low-tube current with iterative model reconstruction on Philips Brilliance iCT Elite FHD in the accuracy of spinal QCT using a European spine phantom. *Quant Imaging Med Surg* 2018;8:32-8.
40. Xiangshu C, Cheng X, Peng J, Li B, Su J, Chunlai D. Assessment of Precision and Accuracy of Spinal QCT in a Multi-centre Clinical Research with a European Spine Phantom. *Chinese Journal of Medical Imaging* 2011;19:912-7.